Supporting Information

A transition-metal-and-solvent-free dual-graphite battery

Minh Canh Vu, Hrishikesh S. Srinivasan, Priyadarshini Mirmira, Emily S. Doyle, Reginaldo J. Gomes, and Chibueze V. Amanchukwu*

Pritzker School of Molecular Engineering, University of Chicago, Chicago, IL 60637, USA.

*Corresponding author: Chibueze V. Amanchukwu. E-mail: chibueze@uchicago.edu.

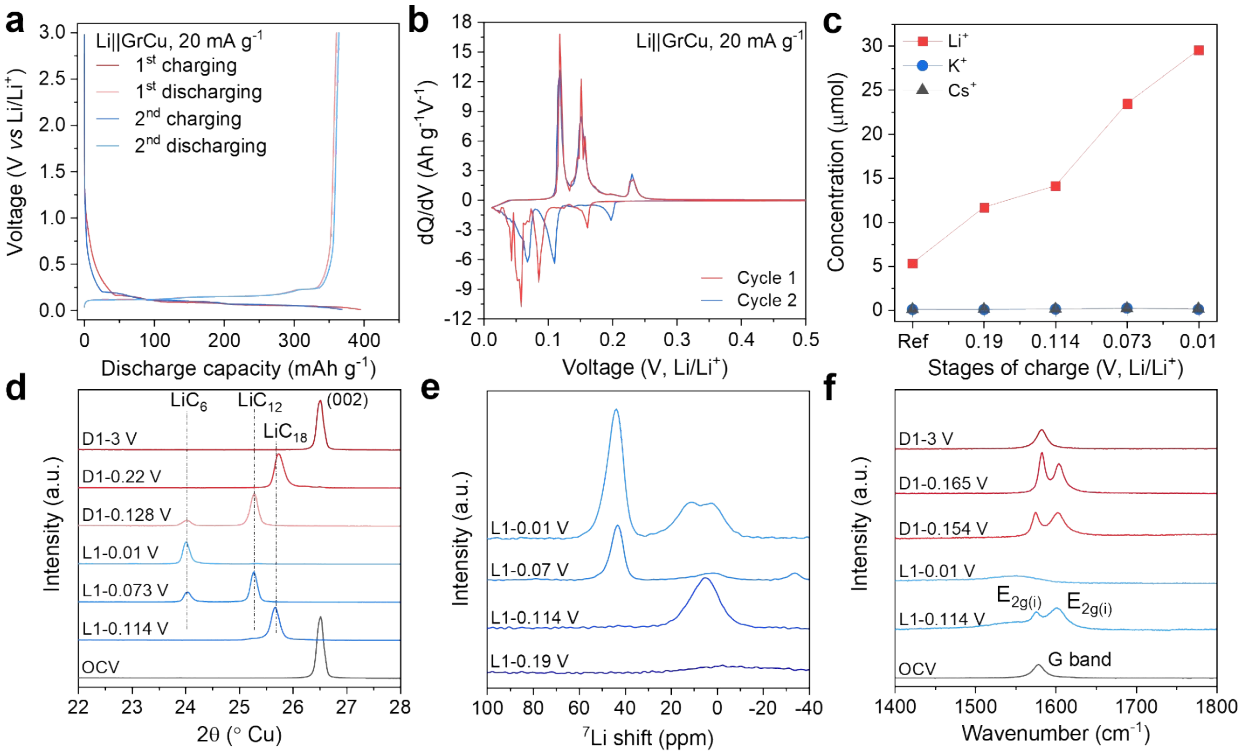

Figure S1. (a) Charge-discharge voltage profiles, (b) dQ/dV curves of Li||GrCu cells using 3M $Li_{0.3}K_{0.35}Cs_{0.35}FSA$/FEC-FEMC electrolyte (LE) at 20 mA g^{-1}. (c) Cation concentrations in the intercalated GrCu electrodes at different states of charge from the Li||GrCu cells using LE at 20 mA g^{-1} obtained using ICP-MS. (d) Ex-situ XRD pattern, (e) solid-state NMR, and (f) Raman spectra of the intercalated GrCu electrodes at different stages of charge from the Li||GrCu cells using LE at 20 mA g^{-1}, respectively.

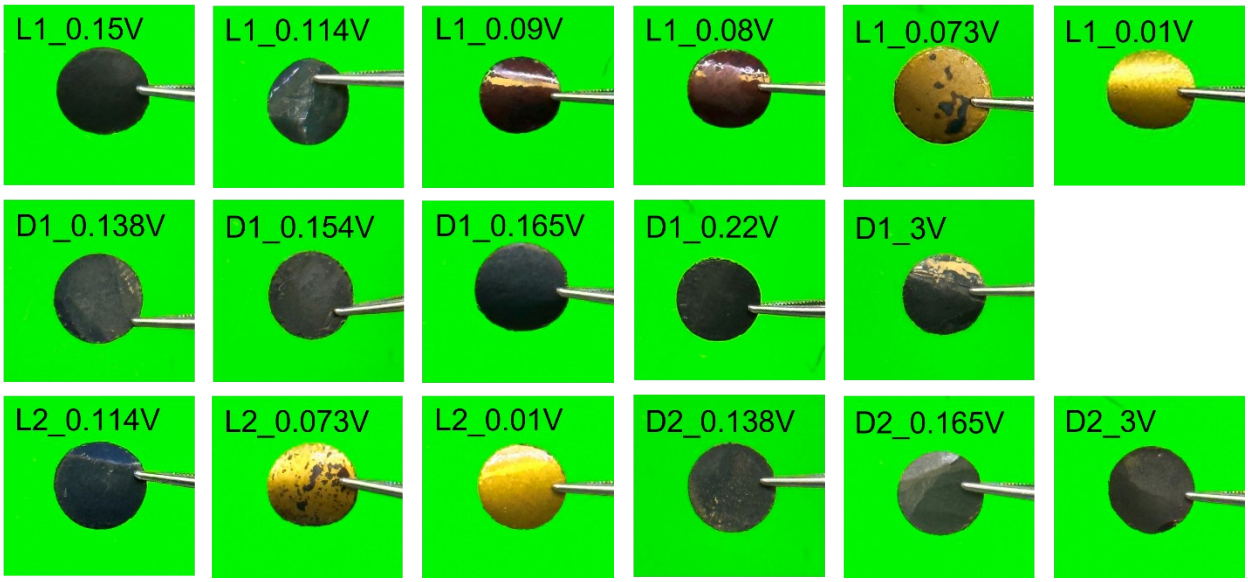

Figure S2. Digital photos of the GrCu electrodes from the Li||GrCu cells at different stages of charge/discharge at 20 mA g^{-1} and 80°C using the molten salt electrolyte (MSE). The names of the samples are represented at the left corner of the images, where L or D means Lithiation (charge) or Delithiation (discharge), followed by the cycle index, and the number after "_" represents the stages of charge/discharge.

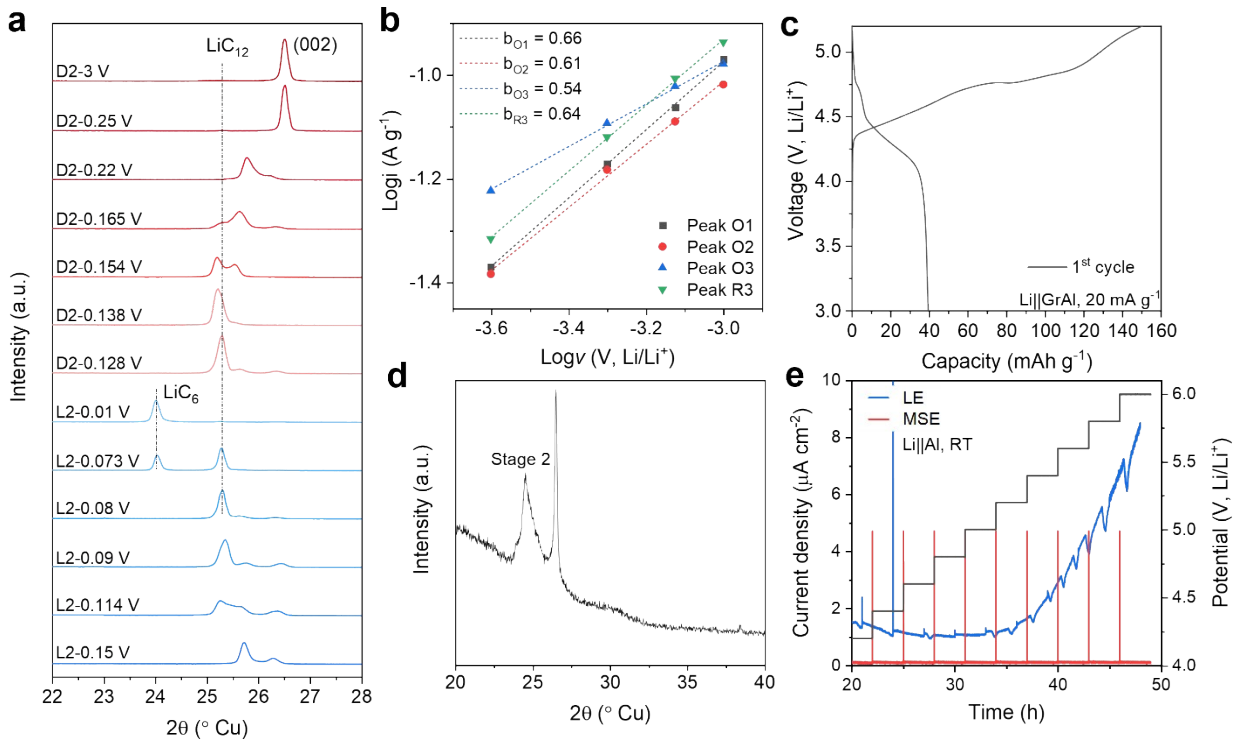

Figure S3. (a) Ex-situ XRD pattern of the intercalated GrCu electrodes at different stages of charge from the Li||GrCu cells using $Li_{0.3}K_{0.35}Cs_{0.35}FSA$ MSE at 20 mA g^{-1}. (b) log*i* versus log*v* to determine *b* values for graphite cathodes. (c) Charge-discharge voltage profile of Li||GrAl cells using LE at 20 mA g^{-1}. (d) Ex-situ XRD pattern of the GrAl electrodes after being charged to 5.2V using LE at 20 mA g^{-1}. (e) Potentiostatic hold from 3-6V (vs. Li/Li^+) of Li||Al cells using MSE (red line) and LE (blue line) with 0.2V steps.

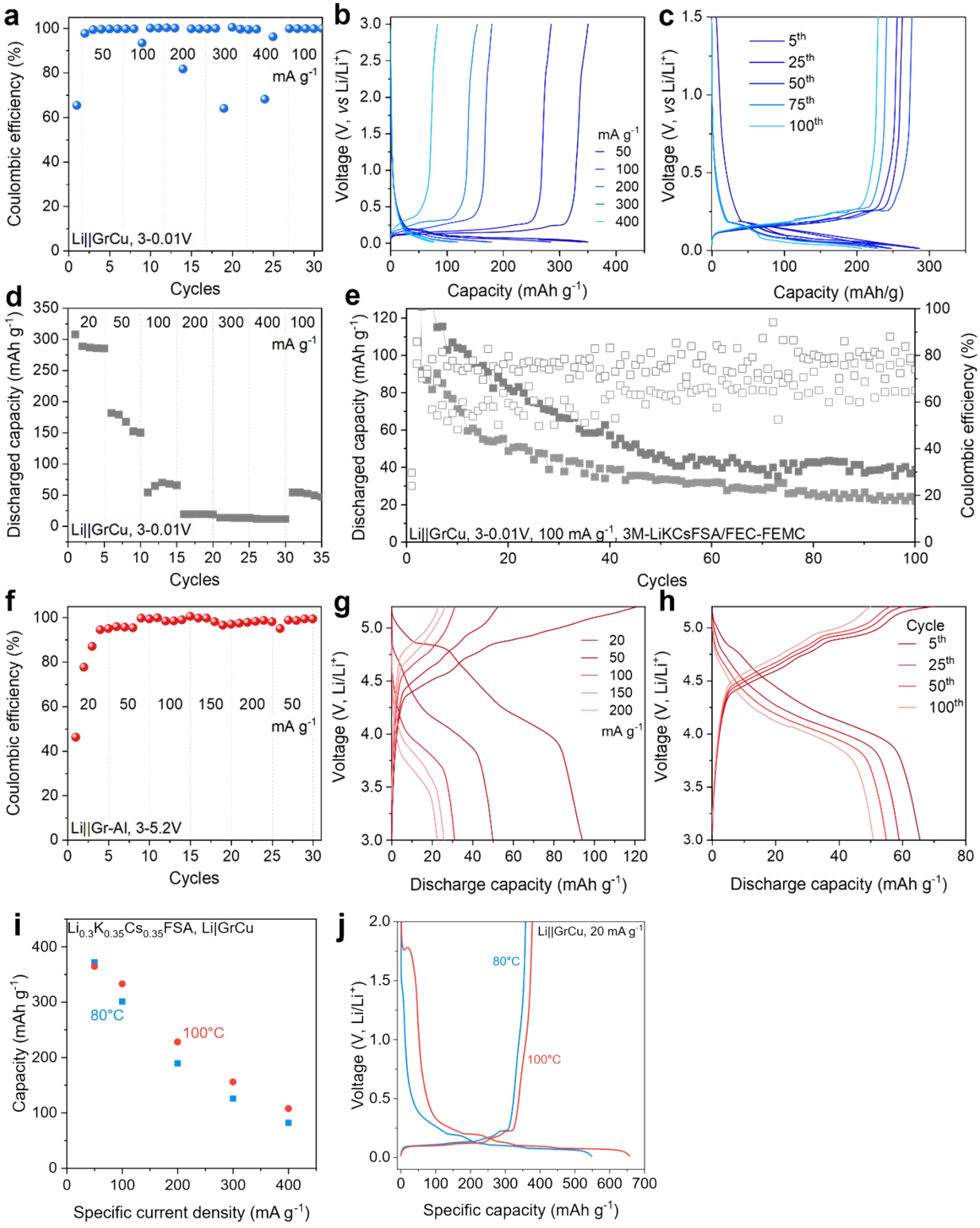

Figure S4. (a) Coulombic efficiency of the Li||GrCu cells using MSE at different current densities in the voltage range of 0.01-3V (vs. Li/Li^+). Selected voltage profiles of the Li||GrCu cells using MSE at (b) different current densities, and (c) different cycles at 100 mA g^{-1}. (d) Discharge capacities of the Li||GrCu

cells using LE at different current densities in the voltage range of 0.01-3V (vs. Li/Li^+). (e) Long-term cycling of Li||GrCu cells using LE at 100 mA g^{-1} in the voltage range of 0.01-3V (vs. Li/Li^+). (f) Coulombic efficiency of the Li||GrAl cells using MSE at different current densities in the voltage range of 3-5.2V (vs. Li/Li^+). Selected voltage profiles of the Li||GrAl cells using MSE at (g) different current densities, and (h) different cycles at 50 mA g^{-1}. (i) Discharge capacities of the Li||GrCu cells using MSE at different temperatures (80 ^oC and 100 ^oC) in the voltage range of 0.01-3V (vs. Li/Li^+). (j) Voltage profiles of Li||GrCu cells using MSE at 80°C and 100°C at 20 mA g^{-1}.

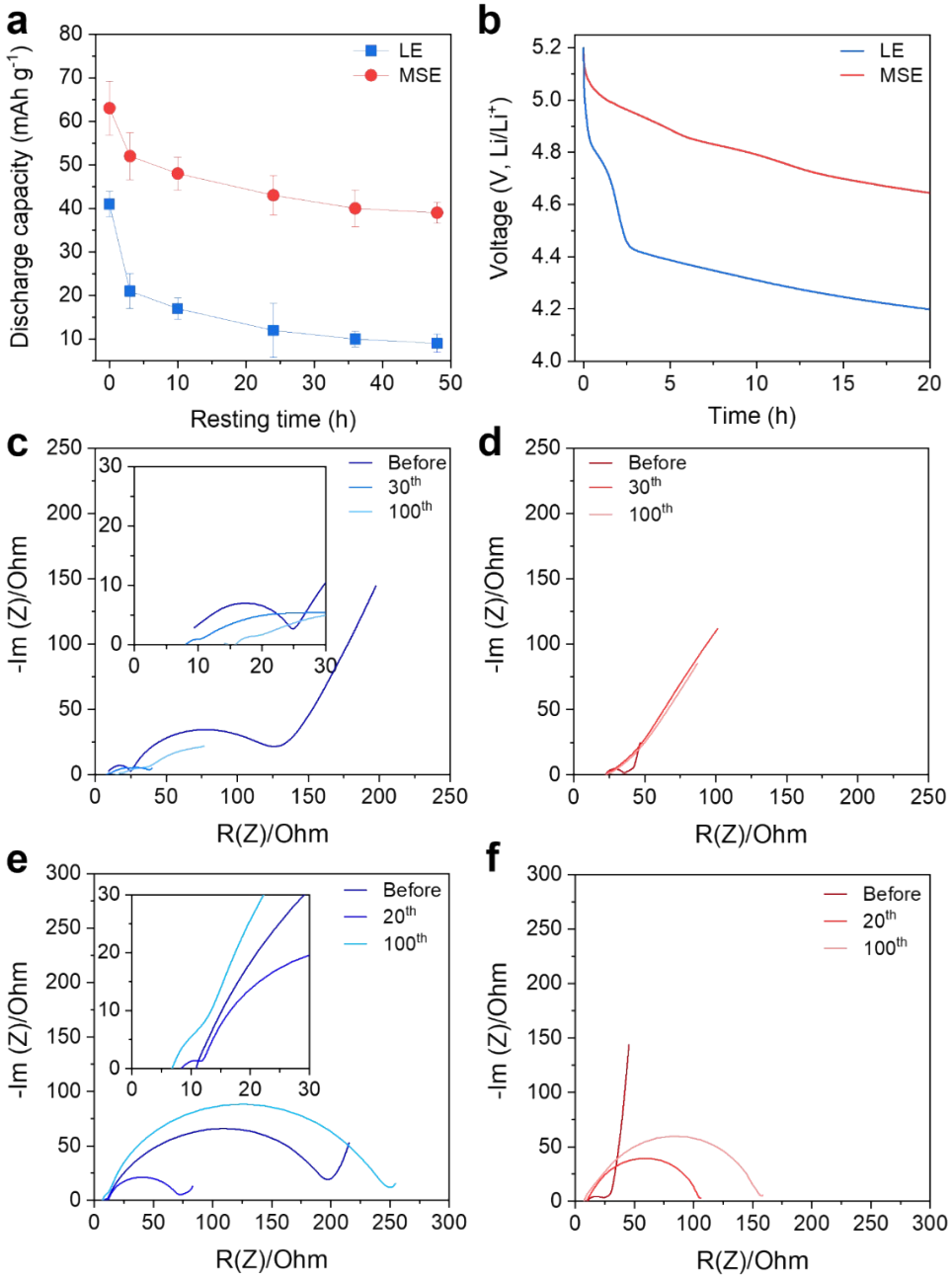

Figure S5. Evolution of (a) discharged capacity and (b) Potential as a function of time of the Li||GrAl cells using MSE and LE. Nyquist plots of the cycled GrCu and GrAl electrodes using (c, e) LE, and (d, f) MSE, respectively.

The rate of self-discharge (r) can be calculated from the following equation:

$$r = \frac{C_t - C_{t'}}{C_t (t - t')} x100\% \qquad \text{(S1)}$$

where C_t and $C_{t'}$ represent the discharge capacities after resting for t and t', respectively.

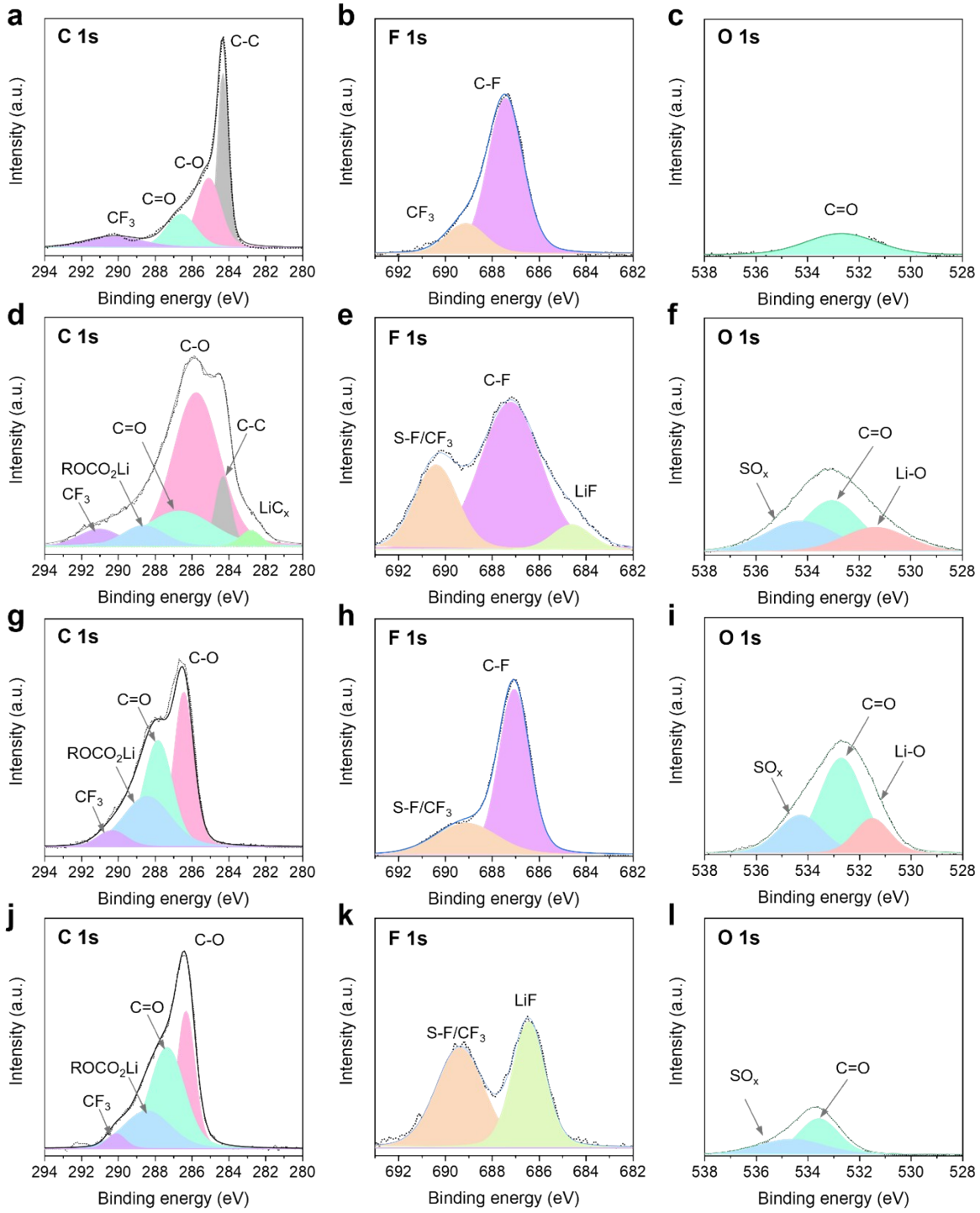

Figure S6. High-resolution XPS spectra of (a-c) C 1s, F 1s, and O 1s of the pristine GrCu electrode, respectively. (d-f) C 1s, F 1s, and O 1s of the GrCu electrode from Li||GrCu cells using LE after formation cycles, respectively. (g-i) C 1s, F 1s, and O 1s of the GrCu electrode from Li||GrCu cells using LE after 100 cycles of lithiation/delithiation, respectively. (j-l) C 1s, F 1s, and O 1s of the GrCu electrode from Li||GrCu cells using MSE after formation cycles, respectively.

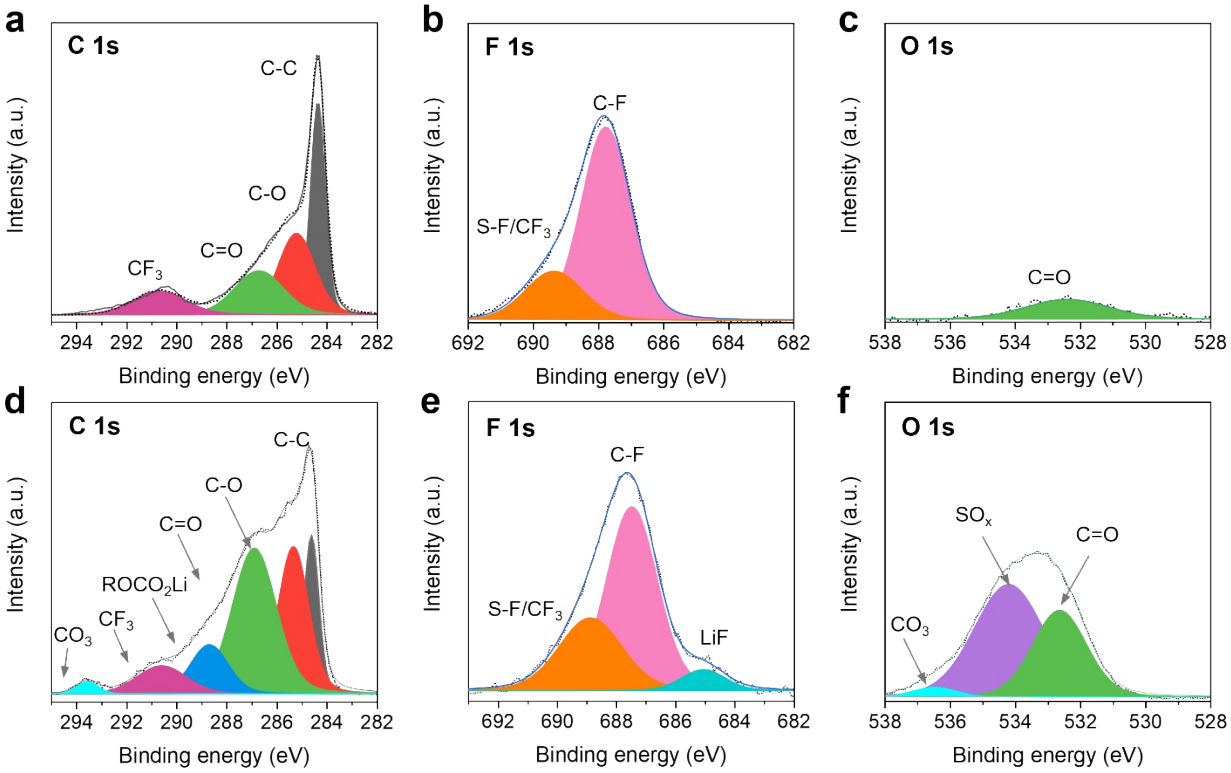

Figure S7. High-resolution XPS spectra of (a) C 1s, (b) F 1s, and (c) O 1s of the pristine GrAl electrode, respectively. (d) C 1s, (e) F 1s, and (f) O 1s of the GrAl electrode from Li||GrAl cells using LE after 100 cycles of FSA^- anion intercalation/de-intercalation, respectively.

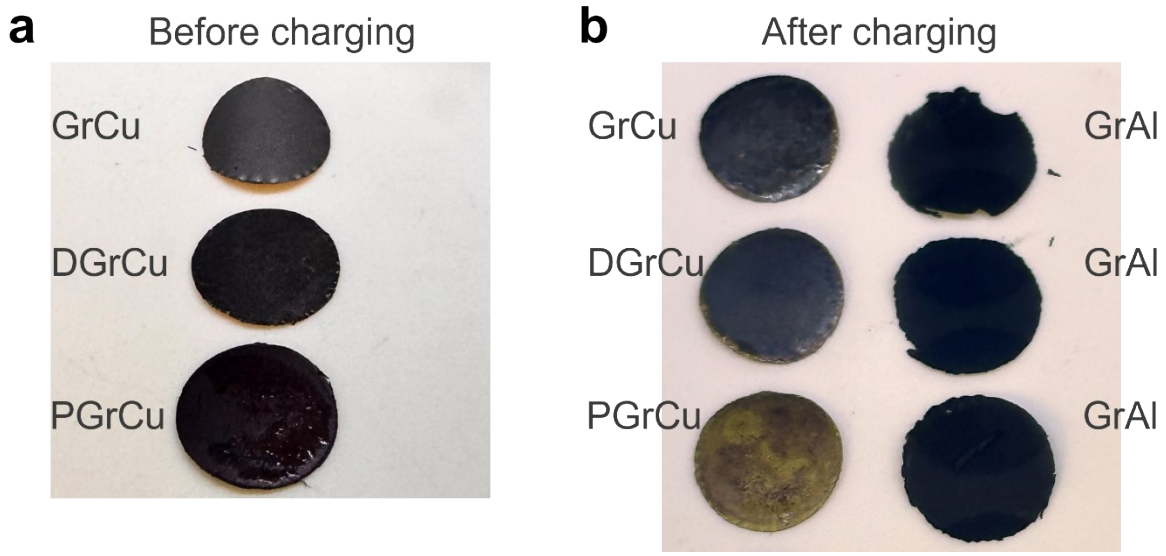

Figure S8. Digital photos of (a) the precycled GrCu before being charged to 5.2V (vs. Li/Li^+), and (b) the precycled GrCu (left-column), and GrAl electrodes (right-column) after being charged to 5.2V (vs. Li/Li^+) using MSE. Before charging, the anode GrCu electrodes underwent 3 formation cycles and then charged to different stages using the Li||GrCu cells including (1) charging to 0.09 V for partially lithiated graphite (PGrCu), (2) discharging to 3 V for fully delithiated graphite (DGrCu) using MSE.

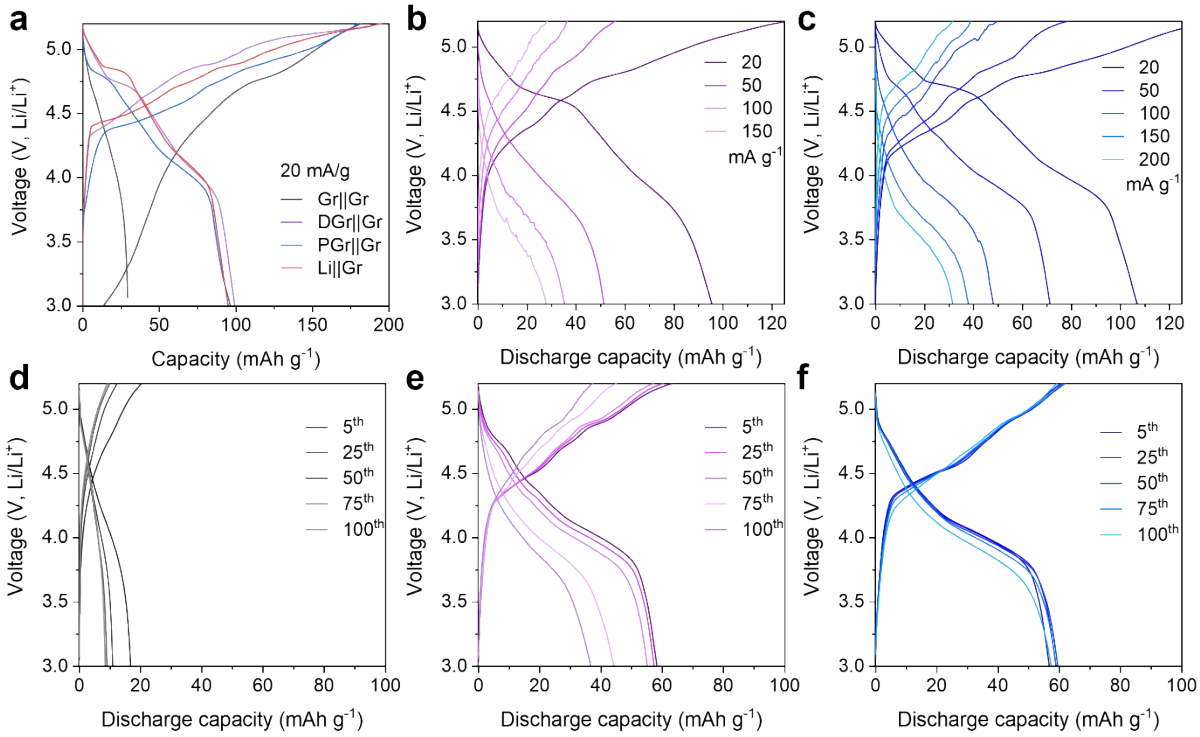

Figure S9. (a) Voltage profiles of the first cycle of different types of full-cell DGB at 20 mA g^{-1} using MSE in the voltage range of 3-5.2V (vs. Li/Li^+). (b-c) Charge-discharge voltage profiles of (b) DGr||Gr cells and (c) PGr||Gr cells using MSE at different current densities in the voltage range of 3-5.2V (vs. Li/Li^+). (d-f) Selected charge-discharge voltage profiles of (d) Gr||Gr, (e) DGr||Gr cells, and (f) PGr||Gr cells using MSE at different cycles at 50 mA g^{-1} in the voltage range of 3-5.2V (vs. Li/Li^+).

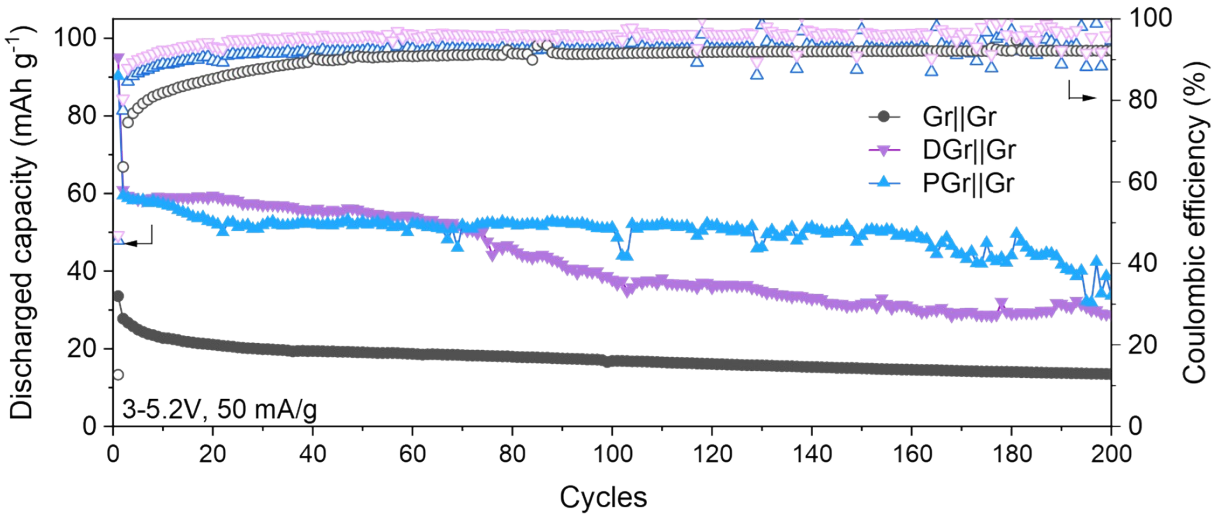

Figure S10. Long-term cycling of the different types of DGB cells using MSE at 50 mA g^{-1} in the voltage range of 3-5.2V (vs. Li/Li^+) up to 200 cycles.

Table S1. Overview of the measurement data (2θ values for the most dominant peaks) and calculated parameters [most dominant stage index (n), periodic repeat distance (I_c), gallery height (d_i), gallery expansion (Δd)] for the operando X-ray diffraction study of FSA-anion intercalation/de-intercalation into/from graphite.

Voltage (V)	2θ(00n+1) (degree)	2θ(00n+2) (degree)	d(00n+2)/d(00n+1)	Stage, n	I_c/Å	d_i/Å	Δd/Å	Δc/%
4.65	23.74	30.01	1.259	3	14.870	8.160	4.805	47.744
4.75	23.74	30.01	1.259	3	14.870	8.160	4.805	47.744
	24.1	31.05	1.282	2	11.507	8.152	4.797	71.493
4.95	24.1	31.05	1.282	2	11.507	8.152	4.797	71.493
	22.4	34	1.505	1	7.901	7.901	4.546	135.496
5.1	22.4	34	1.505	1	7.901	7.901	4.546	135.496
5.2	22.4	34	1.505	1	7.901	7.901	4.546	135.496